MINERALIZATION OF CHEMICALLY TREATED SAWDUST AND ITS USE AS AGGREGATES IN FLY ASH-BASED GEOPOLYMER COMPOSITES

Rui Rosa de Morais Júnior[1,2]

https://orcid.org/0000-0001-6729-6895

Arthur Behenck Aramburu[3]

https://orcid.org/0000-0001-9842-6904

André Luiz Missio[1]

https://orcid.org/0000-0001-9373-6313

Rafael Beltrame[1]

https://orcid.org/0000-0001-6352-0052

Rafael de Avila Delucis[1,♠]

https://orcid.org/0000-0002-3657-9216

Darci Alberto Gatto[1]

https://orcid.org/0000-0002-6805-3243

ABSTRACT

This study presents an innovative approach to wood mineralization through various pretreatments, focusing on the application of chemically treated sawdust as aggregates in fly ash-based geopolymer composites. Eucalyptus wood sawdust underwent five distinct treatments: cold water washing (CWW), hot water washing (HWW), sodium hydroxide washing (SHW), calcium hydroxide mineralization (CHM), and Portland cement mineralization (PCM). Comparative analyses revealed that the properties of these geopolymer composites were comparable to, or exceeded, those achieved with traditional sand aggregate. The incorporation of the pretreated wood aggregates resulted in geopolymer composites with comparable compressive strength values at 30 and 90 days, with further strength improvements after aging especially for composites treated with HWW or SHW. Additionally, these composites exhibit the formation of a mineral layer on the wood surface, confirming successful mineralization. This study concludes that HWW and SHW treatments significantly enhanced the compatibility between wood and the geopolymer matrix, paving the way for developing light weight geopolymer composites with promising applications in the sustainable building materials.

Keywords: Alkaline activation, fly ash, geopolymer composite, mechanical properties, sustainable aggregates, wood sawdust, wood mineralization.

[1]Federal University of Pelotas. Postgraduate Program in Materials Science and Engineering. Pelotas, Brazil.

[2]Federal University of Pampa. Production Engineering. Bagé, Brazil.

[3]Federal University of Rio Grande do Sul. Postgraduate Program in Mining, Metallurgical and Materials Engineering. Porto Alegre, Brazil.

♠Corresponding author: rafael.delucis@ufpel.edu.br

Maderas. Ciencia y tecnología 2025 (27): 13, 1-19

Universidad del Bío-Bío

INTRODUCTION

The escalating generation of industrial waste and its detrimental impact on the environment have raised urgent concerns globally. Among these wastes, fly ash (FA) has emerged as a significant byproduct resulting from the large-scale combustion of coal to produce electricity. Comprising fine particulate matter with a spherical morphology, FA is carried by coal combustion gases and subsequently captured by filters and precipitators (Ahmaruzzaman 2010). Unfortunately, the improper disposal of FA in landfills and mines poses severe environmental and health hazards.

In recent years, extensive research has been dedicated to exploring alternative applications for FA, with particular emphasis on its incorporation in the construction industry, wherein the integration of FA in geopolymers presents a unique opportunity to mitigate the adverse environmental consequences associated with coal burning. In this sense, FA has been used as a binder in geopolymer composites through alkaline activation, leading to the emergence of geopolymers as a promising next-generation composite material (Pavithra *et al.* 2016, Azevedo *et al.* 2017, Amran *et al.* 2021, Danish *et al.* 2022). Furthermore, geopolymers may be used as substitutes for ordinary Portland cement composites is some applications, which also mitigate the CO_2 emissions during cement production (Arslan *et al.* 2019, Gollakota *et al.* 2019, Amran *et al.* 2020).

In this sense, geopolymers are formed through the alkali activation of aluminosilicate precursors, and FA serves as an excellent aluminosilicate source due to its high content of silica (SiO_2) and alumina (Al_2O_3) (Gollakota *et al.* 2019). The reaction between fly ash and an alkaline activator, typically a mixture of sodium silicate and sodium hydroxide or potassium hydroxide, initiates a polycondensation process leading to the formation of a three-dimensional geopolymeric network (Luhar and Luhar 2022).

Concurrently, there has been a surging interest in the utilization of wood waste, especially wood sawdust, as a sustainable and eco-friendly aggregate in composite materials. Wood sawdust exhibits favorable properties such as low cost, low density, high specific strength, and minimal processing energy consumption, making it an attractive candidate for enhancing the mechanical properties of composites (Asante *et al.* 2021, Furtos *et al.* 2021). Despite these inherent advantages, the hydrophilic nature of wood cell walls poses a challenge to effective incorporation of sawdust in composites, as it can result in dimensional instability due to swelling and shrinking under humid conditions (Asante *et al.* 2022). Additionally, the alkaline nature of the matrix in composites can lead to wood degradation, causing concerns over long-term durability and the presence of common wood compounds, such as extractives and carbohydrates, may interfere with the curing process of the matrix, limiting the full potential of sawdust as an aggregate (Fan *et al.* 2012).

To overcome these challenges and fulfill the growing demand for sustainable materials, researchers have diligently pursued various wood surface treatment strategies, including washing, immersion, and mineralization techniques. These treatments are aimed at enhancing the compatibility between wood particles and alkaline matrices, thereby improving the overall performance and properties of wood-based composites. (Jorge *et al.* 2004, Asante *et al.* 2022). Among these treatments, mineralization has emerged as a particularly promising approach and involves the in situ introduction of minerals within the wood structure without creating chemical bonds, thereby facilitating enhanced interfacial adhesion with the alkaline matrix (Maichin *et al.* 2020).

While there have been significant advancements in the mineralization of wood particles for composite applications, a notable research gap remains concerning the specific mineralization of particles intended for use in geopolymer composites (Malenab *et al.* 2017, Boadu *et al.* 2018, Lazorenko *et al.* 2020, Maichin *et al.* 2020). Bridging this knowledge gap, this study aims to enhance the compatibility between mineralized wood sawdust and the geopolymer matrix through the mineralization of sawdust particles with fly ash and either alkaline washing or water washing, elucidating the chemical mechanisms and interactions involved in the mineralization process. The ultimate goal is to harness the potential of mineralized sawdust as aggregates in geopolymer composites, paving the way for the development of high-performance, sustainable, and eco-friendly construction materials.

Mineralization of chemically treated sawdust..: Morais Júnior *et. al*

Maderas. Ciencia y tecnología 2025 (27): 13, 1-19

MATERIALS AND METHODS

Raw materials

Fly ash (FA) utilized in this study was originated from a power plant (CGT Eletrobras) located in Candiota/Brazil, that disposes its ashes in landfills, and supplied by Companhia Riograndense de Mineração. Eucalypt wood sawdust was obtained from a local lumber company located in Bagé/Brazil.

FA, sawdust and sand were oven dried at 60 °C for 3 h to ensure optimal moisture content, subsequently, the sawdust and sand were sieved to obtain granulometry within the range suitable for fine aggregates, adhering to the ABNT NBR 7211-05 (2005) standard, while FA was sieved through a #2,62 mm mesh sieve to eliminate impurities and larger granulometry particles. All the refined materials were stored in impermeable polymeric containers to maintain their integrity.
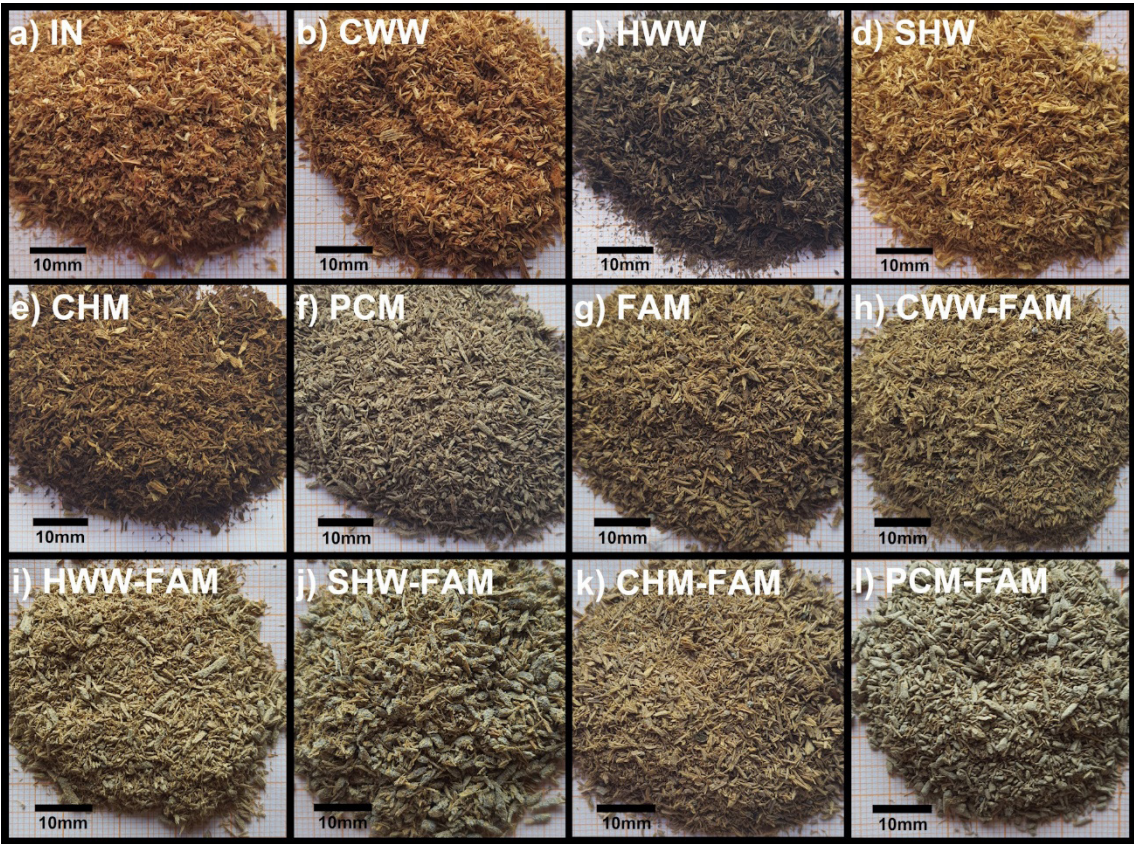
Sawdust pretreatments

The parameters employed for each pretreatment applied to the untreated sawdust (IN) are presented in Table 1. Subsequent to these procedures, the mixtures of sawdust and corresponding liquids from cold water washing (CWW), hot water washing (HWW), and sodium hydroxide washing (SHW) pretreatments were passed through a #0,21 mm sieve to retain the sawdust and then air-dried. For calcium hydroxide mineralization (CHM) and Portland cement mineralization (PCM) pretreatments, the mixture remained in the mixer for 24 h before being removed for air-drying. Following a 30-day air-drying period, the untreated IN sawdust was further dried in an oven and sieved using the same procedure as described earlier. This meticulous approach ensured minimal discrepancies in granulometry and moisture content between the pretreated sawdust and the untreated IN sawdust. The experimental design and the chemical treatments applied to the untreated (IN) sawdust wood are detailed in Table 1. The different treatments and their combinations provided differences in the color of the wood sawdust shown in Figure 1.

Table 1: Experimental design and chemical treatments applied to the untreated (IN) sawdust wood.

Pretreatments	Proportions	Procedure
Cold water washing (CWW)	Sawdust/potable water 1/8 (volume)	Wood sawdust immersed in potable water at room temperature for 24 h
Hot water washing (HWW)	Sawdust/hot water 1/8 (volume)	Wood sawdust immersed in potable water at 90±5 °C for 24 h
Sodium hydroxide washing (SHW)	Sawdust/NaOH solution 1/20 (mass)	Wood sawdust immersed in 1 % NaOH solution for 24 h
Calcium hydroxide mineralization (CHM)	$Ca(OH)_2$/sawdust/water 1/20/20 (mass)	Wood sawdust mixed with calcium hydroxide with 60 clockwise and 60 counterclockwise rotations at 20 rpm. After adding deionized water, five additional rotation cycles were performed with 30-min intervals between each cycle.
Portland cement mineralization (PCM)	Sawdust/cement 5:1 (volume) and sawdust/deionized water 1:1 (mass)	Wood sawdust mixed with Portland cement with 60 rotations clockwise and 60 rotations counterclockwise at 20 rpm. Deionized water was then added, followed by another rotation cycle at 20 rpm.

Maderas. Ciencia y tecnología 2025 (27): 13, 1-19

Universidad del Bío-Bío

Figure 1: Photographs illustrating the visual changes in sawdust samples before and after treatments. Untreated sawdust (IN) (a) treated samples include cold water washing (CWW) in (b) hot water washing (HWW) in (c) sodium hydroxide washing (SHW) in (d) calcium hydroxide mineralization (CHM) in (e) and Portland cement mineralization (PCM) in (f) sawdust treated with fly ash (FAM) appears in (g), followed by combinations of FAM with CWW (h) HWW (i) SHW (j) CHM (k) PCM (l).

Characterization of the raw materials

Sand, FA, and wood sawdust surfaces underwent analysis using scanning electron microscopy (SEM) combined with energy-dispersive X-ray spectrometry (EDS) on a JEOL JSM-6390 instrument, with adjusted working voltages ranging from 10 kV to 15 kV. X-ray diffraction (XRD) analysis of the FA was conducted using a Rigaku Ultima IV diffractometer with Cu–Kα radiation (λ= 1,5418 Å) at an accelerating voltage of 40 kV. The diffracted beam was scanned in 0,01° steps for 2 s within an angular range from 10 to 70º 2θ. Crystallinity index was calculated by dividing the area below the crystalline peaks by the total area below the diffractogram line, as recommended in the literature (Yang *et al.* 2019). Its composition was determined by the Rietveld method using X'Pert HighScore software. The granulometric distribution of the FA was analyzed via laser diffraction using Shimadzu model CILAS 1190 operating in a range from 0,04 to 2500 µm and a wavelength of up to 830 nm. Moreover, wood sawdust and sand granulometries were determined by the pass of the material through sieves (4,75; 2,36; 1,18; 0,6; 0,3 and 0,15 mm).

Specific gravity and unit specific gravity of the FA, sand and sawdusts were calculated according to procedures described in ABNT NBR NM 52-03 (2003) and ABNT NBR NM 45-06 (2006) standards. Measurements of wavelength-dispersive X-ray fluorescence (WD-XRF) and loss on ignition (LOI) were performed using a PANalytical AXIOS Minerals WD-XRF instrument equipped with a 4 kW Rh anode Super Sharp X-ray Tube and NBR NM 18 standard, respectively.

Mineralization of chemically treated sawdust..: Morais Júnior *et. al*

Maderas. Ciencia y tecnología 2025 (27): 13, 1-19

Mineralization processes

Sodium hydroxide (NaOH, 99 %, Quimidrol Ltda) and sodium silicate (Na_2SiO_3, Quimidrol Ltda) were used to produce a commonly used alkaline activator solution (AAS) (Pavithra *et al.* 2016). To avoid heating during dissolution in deionized water, which could negatively affect geopolymerization reactions, NaOH and Na_2SiO_3 were dissolved in for 24 h and 3 h, respectively. The NaOH molarity and the Na_2SiO_3/NaOH mass ratio were fixed at 14 M and 1,5, respectively, as recommended by the literature (Asante *et al.* 2021).

The alkaline activation process started with the mixture of untreated sawdust (IN) and FA in a 1:1 mass ratio using 60 clockwise rotations and 60 counterclockwise rotations at 20 rpm. Afterwards, the AAS was added at a 0,65 AAS/FA mass ratio and the mixture continued for nine more rotation cycles at 20 rpm. This same method was applied for the CWW, HWW, SHW, CHM, and PCM-treated sawdust woods. Thereafter, these aggregates incorporated with FA are called as CWW-FAM, HWW-FAM, SHW-FAM, CHM-FAM, PCM-FAM for the sawdusts treated by cold water washing, hot water washing, sodium hydroxide washing, calcium hydroxide mineralization and Portland cement mineralization, respectively.

Manufacturing of the composites

Following the same formulations used in the geopolymer's manufacturing, the following ratios were adopted: an aggregate/FA volume ratio of 12:20, an AAS/FA mass ratio of 13:20, and a water/FA ratio of 1:10.

Before the mixing process, the aggregates (sand and sawdust) and the FA were oven-dried at 60-80 ºC for 24 h and stored in plastic bags. The mixing procedure started by manual stirring of the aggregate and FA for 60 s into a 2 L beaker. Then, AAS and deionized water were added and mixed for an extra 180 s. This mixture was poured into polymer molds and demolded prior to the characterization tests, except the cylindrical specimens with dimensions of 2,1 cm × 10 cm (diameter × length), which were oven-dried at 60 ºC for 24 h before demolding since it was difficult to demold them at room temperature.

Characterization of the composites

Water absorption (WA), apparent porosity (AP), and dry bulk density (DBD) were measured using the known equations available in the literature (Asante *et al.* 2021). Cylindrical specimens with dimensions of 2,7 cm × 4,9 cm (diameter × length), cured for 28 days, remained immersed in water for 72 h at room temperature and then dried at 105 °C until reaching a constant mass.

Compressive tests were carried out for specimens with the cylindrical dimensions of 2,7 cm × 4,9 cm (diameter × length) at the ages of 28 and 90 days. The tests were performed using an EMIC DL 10000 universal testing machine equipped with a 100 kN load cell at a 1 mm/min cross head speed, as recommended by ABNT NBR 7215-19 (2019) standard.

Three-point bending tests were performed at 28 days old cylindrical specimens with dimensions of 2,1 cm × 2,1 cm × 10 cm. The tests were conducted using a span length of 80 mm and a speed movement of 1 mm/min at the midpoint. Additionally, a 20 kN load cell was implemented in the same equipment used for the compressive tests. The load vs. displacement curves were used to calculate modulus of rupture (MOR) and modulus of elasticity (MOE), according to the recommendation of ASTM C674-99 (1999) standard. All physical and mechanical tests were conducted using four samples per group.

Burning tests were adapted from the procedures described by Underwriters Laboratories 94 (UL94). The horizontal burn test was performed on the broken specimens that came from the bending tests. The flame was placed onto the specimen and kept for 10 s, and after 180 s, the flame was placed for another 10 s and then removed again. The duration of the flame after its removal from the flame source was observed after both the first and second application.

Thermogravimetric analysis (TG) was performed to analyze the thermal stability of geopolymer composites using one sample per group. This analysis was performed on a 4 g powder sample, which was obtained by maceration from a small broken specimen. The analysis was carried out in a temperature range between 25 ºC and 1000 ºC with a constant heating rate of 10 ºC/min under a constant inert nitrogen atmosphere and a flow rate of 1 L/min. For this, a TGA-1000 Navas Instrument was used. A platinum crucible

Maderas. Ciencia y tecnología 2025 (27): 13, 1-19

Universidad del Bío-Bío

was used for all TGA measurements to minimize interference and ensure consistent thermal properties.

Fragments from the compressive tests were analyzed for morphological features by SEM equipped with an energy dispersion spectroscopy (EDS) probe using the aforementioned equipment and parameters, with images captured at magnifications of 100x and 1000x and a working voltage of 20 kV. Other fragments were milled in a ring mill for 120 s, and the resulting powders were analyzed by XRD to calculate crystallinity index (C). For that, a Bruker D8 desktop diffractometer, configured with CuKα$_{1,2}$ radiation ($\lambda_1 = 0,15406$ nm, $\lambda_2 = 0,15444$ nm) with 5 ° opening. Operating conditions were set to 40 kV and 40 mÅ, goniometer measurement circle 283 mm, primary optics with 0.4 mm fixed slit, 2,5 ° soller slits, and using Ni-filter in secondary optics. The samples were prepared in standard steel sample holder using a glass plate for a side-loading technique. All samples were measured from 10º to 70º (2θ) with a 0,02 step size and a measurement time of 2 s/step.

Accelerated aging tests (AAT) were performed using a BASS-UUV-STD-SPRAY-4400/2013 artificial weathering chamber. The chamber simulates the effects of degradation caused by sunlight, rain, and dew. The specimens were exposed to alternating cycles of radiation, humidity, and temperature, controlled in accordance with the specifications of ASTM G154-23 (2023) standard. Each sample was exposed to 60 12-hour cycles, totaling 720 h (30 days). These aged specimens were then tested for compression under the aforementioned conditions.

The data underwent ANOVA tests, and whenever the null hypothesis was rejected, Tukey tests were employed to compare the means. Prior to that, both homogeneity of variances and data normality were assessed using Levene and Shapiro-Wilk tests, respectively. All statistical analyses were conducted at a significance level of 5 %.

RESULTS AND DISCUSSION

Sawdust pretreatment effects

The images in Figure 2 confirm the irregular shape of the sand and the spherical shape of the fly ash, which are well-documented in the literature (Garcez *et al.* 2016, Sarmin and Welling 2016). The abbreviations introduced in the Materials and Methods section, such as FA (fly ash), SHW (sodium hydroxide washing), and CHM (calcium hydroxide mineralization), are used throughout the R&D section to maintain consistency. When comparing the untreated sawdust (shown in Figure 3a) with the chemically treated ones that underwent aqueous extractions (Figure 3b, Figure 3c, and Figure 3d), the latter showed a porous structure with surface holes. The pores from the CHM sample (Figure 3e) appear to be covered by a thin mineral layer, likely formed by the reaction of calcium hydroxide with water. The sawdust treated with PCM (Figure 3f) exhibited a rigid layer with surface holes formed by the alkaline hydrolysis induced by the cement hydration. The sawdusts mixed with FA (Figure 3g, Figure 3h, Figure 3i Figure 3j) displayed spherical FA particles fixed on surface mineral layers (highlighted by arrows). Both the CHM-FAM (Figure 3k) and PCM-FAM (Figure 3l) also showed a few spherical FA particles on the surface, which appeared to have a more regular shape compared to the other sawdust woods.
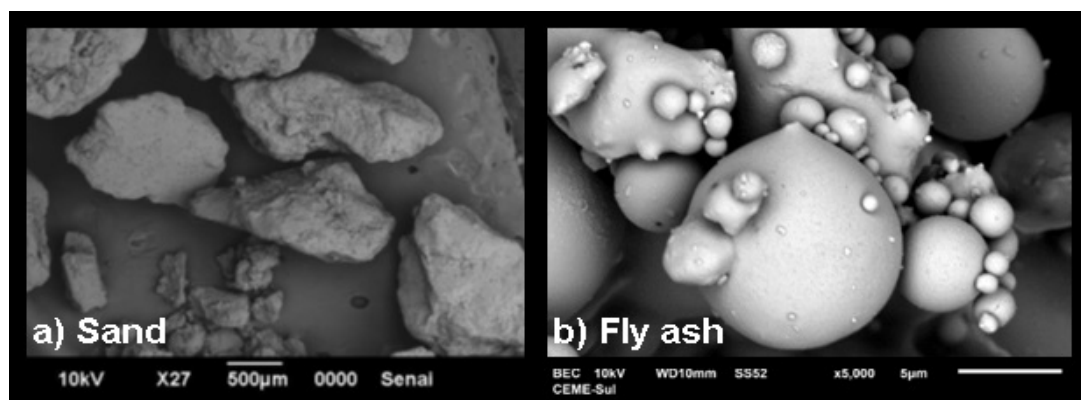
Figure 2: SEM images of the sand (a) and FA (b).
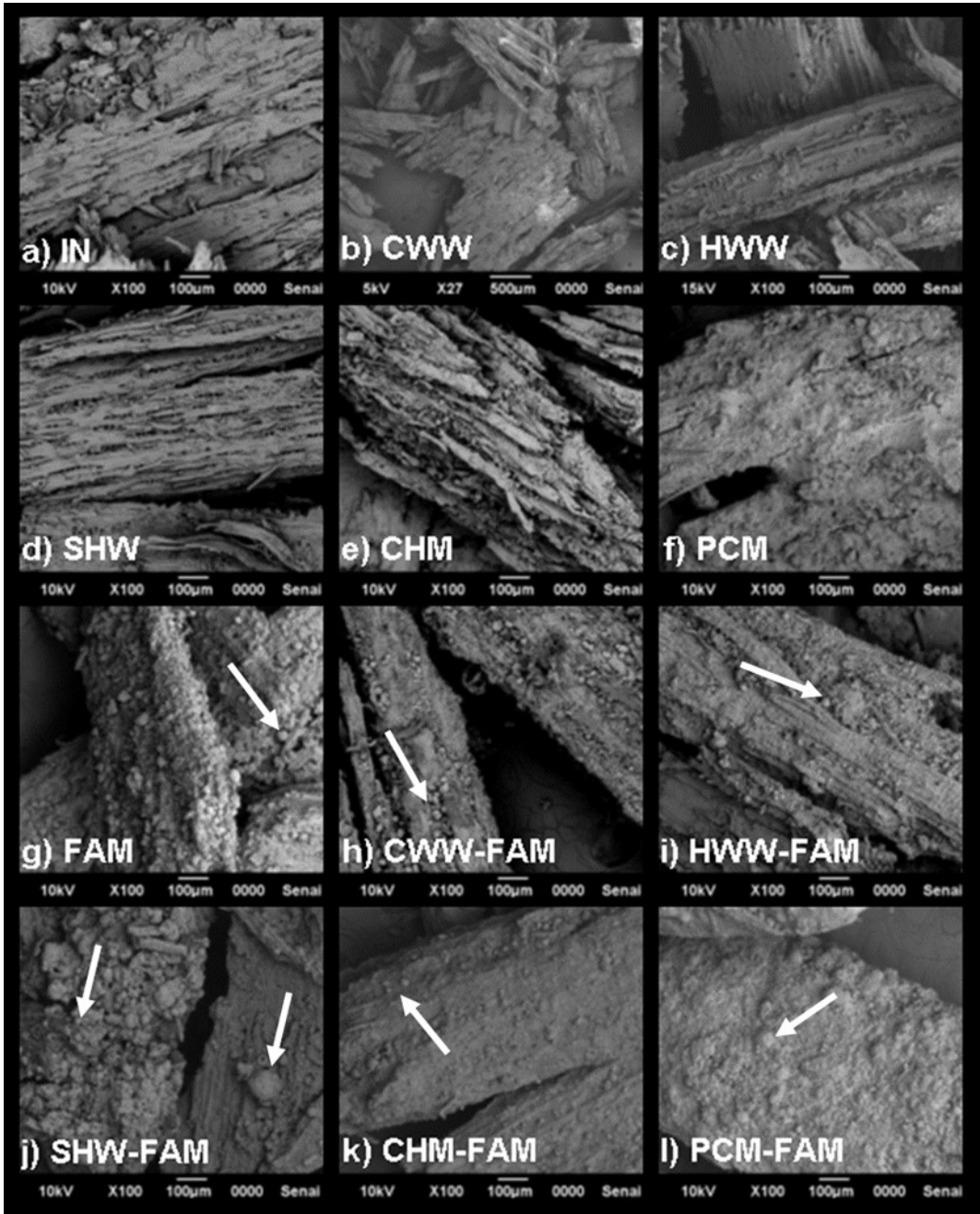
Figure 3: SEM images showing the morphological characteristics of sawdust samples before and after various pretreatments. Untreated sawdust (IN) is displayed in (a). Pretreated sawdust samples include cold water washing (CWW) in (b), hot water washing (HWW) in (c), sodium hydroxide washing (SHW) in (d), calcium hydroxide mineralization (CHM) in (e), and Portland cement mineralization (PCM) in (f). Mineralized sawdust combined with fly ash (FAM) is shown in (g), followed by combinations of fly ash with CWW (h), HWW (i), SHW (j), CHM (k), and PCM (l).

Figure 4 shows the XRD diffractogram of the FA, with the identification of the quartz (COD 96-500-0036), mullite (COD 96-900-1568), and hematite (COD 96-101-1268) phases based on diffraction patterns found in the Crystallography Open Database (COD). The presence of quartz and mullite in the FA corroborates the findings of other authors who have analyzed similar FA-based powders (Manique *et al.* 2017). The calculated crystallinity index of 32 % indicates the high suitability of the FA for use as a binder in geopolymer composites, and this value is consistent with those reported by (Cardoso *et al.* 2015). The chemical composition of the FA comprises 53,7 % quartz, 45,1 % mullite, and 1,2 % hematite, respectively.
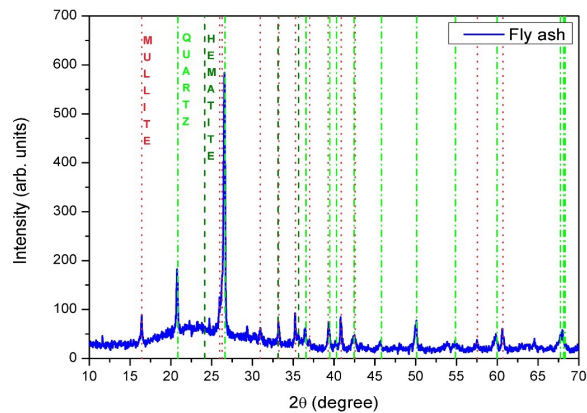
Maderas. Ciencia y tecnología 2025 (27): 13, 1-19

Universidad del Bío-Bío

Figure 4: XRD of the FA.

Table 2 presents the data on the granulometry of the aggregates. The Fineness Modulus (FM) of both the sand and PCM-FAM falls within the optimal zone range of 2,20-2,90 ABNT NBR 7211-05 (2005) standard, while all other samples are in the upper usable zone (2,90 to 3,50), except for SHW. This occurred because 39,63 % of the SHW sample was retained on the 2,36 mm sieve, while the percentage of retention on this sieve was between 0 and 5,49 % for all the other samples. The SEM image of the SHW sawdust, shown in Figure 3d, exhibits large pores, which may indicate cell wall dilation. In fact, the SHW treatment is known to dilate wood fibers, and the immersion of wood in this solution releases new adsorption sites on the surface due to the removal of organic extractives (Sciban *et al.* 2006). Also, the SHW treatment removes organic extractives, including hemicellulose, which expands cell walls and increases surface porosity, creating new adsorption sites (Ravindran and Jaiswal 2016). FA, when combined with these treated surfaces, contributes to the formation of mineral layers through the reaction of aluminosilicate compounds, possibly enhancing interfacial bonding with the geopolymer matrix (Tchadjie and Ekolu 2018).

Table 2: Accumulated retention on sieves and MF.

Material	Sieve sizes (mm)						Bottom	Fineness modulus (FM)
	4,75	2,36	1,18	0,6	0,3	0,15		
Sand (%)	0	4,07	27,79	67,45	89,25	99,2	100	2,88
IN (%)	0	1,00	27,07	76,34	91,44	98,99	100	2,95
CWW (%)	0	0,16	37,28	83,90	94,48	99,27	100	3,15
HWW (%)	0	0	21,20	81,58	92,80	98,85	100	2,94
SHW (%)	0	39,63	70,36	93,59	97,72	99,73	100	4,01
CHM (%)	0	2,41	45,18	85,95	94,47	98,66	100	3,27
PCM (%)	0	3,72	55,12	87,12	92,85	95,77	100	3,35
FAM (%)	0	0,45	41,21	83,57	93,76	98,85	100	3,18
CWW-FAM (%)	0	0,08	29,36	80,53	89,68	98,24	100	2,98
HWW-FAM (%)	0	0,68	43,93	84,82	92,98	97,95	100	3,20
SHW-FAM (%)	0	5,49	42,09	82,34	92,39	99,03	100	3,21
CHM-FAM (%)	0	0,08	35,51	82,62	93,81	99,47	100	3,11
PCM-FAM (%)	0	0,68	13,34	69,36	90,67	99,64	100	2,74

Mineralization of chemically treated sawdust..: Morais Júnior *et. al*

Maderas. Ciencia y tecnología 2025 (27): 13, 1-19

The grain size curve of FA indicates that 100 % of its particles are higher than 0,04 µm and smaller than 600 µm. The following separatrix measures related to the distribution of these values were obtained: D10, D50, and D90 of 5,67 µm, 46,01 µm, and 161,44 µm, respectively, which indicate the percentage of particles with diameters below 10 %, 50 %, and 90 %. Furthermore, the FA exhibited an average diameter of 67,41 µm, which is consistent with the values found in literature (Ahmaruzzaman 2010).

Mineralization processes

Table 3 presents the specific gravity and unit specific gravity of FA, sand, and sawdust woods. The comparison of values reveals that sand exhibits the highest specific gravity, followed by PCM-FAM. The higher specific gravity of PCM-FAM sawdust, in comparison to the other mineralized sawdust woods, indicates a higher amount of added mineral mass on the surface of this sawdust. This observation suggests that the PCM-FAM sawdust has undergone significant mineralization, which can enhance its suitability as a potential lightweight aggregate in geopolymer composites. Additionally, FAM exhibited the lowest specific gravity values, signifying a lower volume for this sawdust, likely due to the effective adhesion of FA to its surface pores. This adhesion could contribute to the increased strength and stability of composites containing FAM. The correlation between specific gravity values and SEM images supports these findings, indicating that the mineralization process affects the characteristics of the sawdust.

Table 3: Specific gravity and unit specific gravity of the non-mineralized and mineralized sawdust woods.

Material	Specific gravity (kg/m³)	Unit specific gravity (kg/m³)
Fly ash	2030 ± 150	830 ± 90
Sand	2810 ± 390	1540 ± 60
IN	1620 ± 120	170 ± 20
CWW	1220 ± 70	170 ± 10
HWW	1740 ± 60	170 ± 10
SHW	1460 ± 140	190 ± 20
CHM	1850 ± 50	220 ± 20
PCM	1790 ± 140	420 ± 40
FAM	1050 ± 90	310 ± 30
CWW-FAM	1730 ± 130	320 ± 40
HWW-FAM	2060 ± 160	410 ± 40
SHW-FAM	2170 ± 130	440 ± 40
CHM-FAM	1750 ± 220	360 ± 40
PCM-FAM	2510 ± 30	640 ± 40

Furthermore, the unit specific gravity of all the sawdusts does not reach 50 % of the value found for sand. Moreover, the non-mineralized sawdusts (IN, CWW, HWW, and SHW) present unit specific gravities below 200 kg/m³, implying their lightweight nature. Among the mineralized sawdust woods, CHM demonstrates the smallest values, followed by FAM. These lower unit specific gravity values in the mineralized sawdust woods, especially in CHM and FAM, are promising indicators of their potential application as lightweight aggregates in geopolymer composites. This aligns with previous studies that have shown the benefits of using mineralized wood waste as an alternative to conventional aggregates in eco-friendly construction materials (Ranjbar and Zhang 2020).

Figure 5 displays the mineralogical composition and LOI values. The graph shows that sand and FA are rich in SiO_2, with contents of 90,51 % and 64,95 %, respectively. These high SiO_2 contents indicate that both sand and FA can contribute significantly to the geopolymerization process and the overall strength of the composites (Ye *et al.* 2018, Maichin *et al.* 2020, Asante *et al.* 2022). Similarly, the mineralized sawdusts also show substantial SiO_2 contents ranging from 18 % to 44 %, indicating their potential reactivity and geopolymerization capacity. However, the CHM-FAM sawdust exhibits a negligible amount of SiO_2 (0,23 %), likely because the primary mineralizing compound is CaO. This suggests that CHM-FAM might have a different

Maderas. Ciencia y tecnología 2025 (27): 13, 1-19

Universidad del Bío-Bío

geopolymerization mechanism compared to the other mineralized sawdust woods.
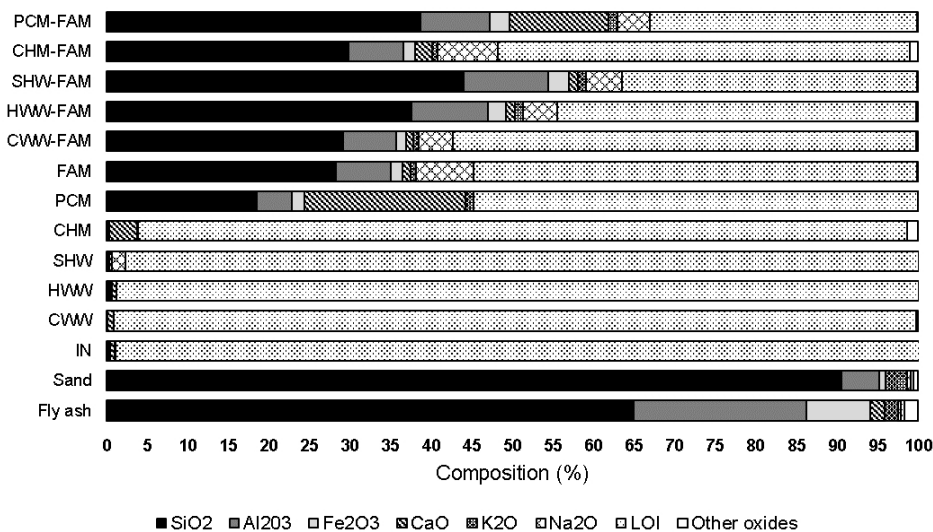
Figure 5: Mineralogical composition of the FA, sand and treated sawdust woods.

The low CaO content (3,48 %) in CHM-FAM is consistent with its high LOI value (94,77 %). However, a high LOI value in CHM-FAM indicates the presence of a significant amount of organic matter that might not have undergone full combustion during the mineralization process. This may require further optimization to enhance the properties of CHM-FAM-based composites.

The SEM images in Figure 3 also support the differences observed in mineralized sawdust woods. The mineral layer formed on the CHM sawdust surface due to the $Ca(OH)_2$ dispersed in water appears thinner than the mineralized layers in the other sawdust woods. This may influence the mechanical properties and durability of the CHM-FAM composite. Therefore, a comprehensive study on the effects of varying mineralizing compounds and processing parameters on the properties of mineralized sawdust-based geopolymer composites would be valuable.

Finally, the non-mineralized sawdusts (i.e., IN, CWW, HWW, and SHW) exhibited high LOI values above 97 %, which was expected since these samples were not mineralized, as shown in the SEM images in Figure 3. These findings suggest the need for mineralization to improve the properties of sawdust and to enhance their potential as sustainable lightweight aggregates in geopolymer composites.

Characteristics of the composites

Table 4 presents the average results for WA (water absorption), AP (apparent porosity), DBD (dry bulk density), MOR (modulus of rupture), and MOE (modulus of elasticity) measured on 28-day-old specimens. The GSAN geopolymer exhibited the highest DBD and the lowest WA and AP, which was expected given that sand has a higher unit specific gravity and lower bulk hydrophilicity, especially when compared to the sawdust woods.

Mineralization of chemically treated sawdust..: Morais Júnior *et. al*

Maderas. Ciencia y tecnología 2025 (27): 13, 1-19

Table 4: Physical and mechanical properties of the composites.

| Specimens	WA (%)	AP (%)	DBD (kg/m³)	MOR (MPa)	MOE (MPa)
GSAN	9,05 c ± 1,21	15,90 b ± 1,95	1780 a ± 50	4,77 ab ± 0,42	3613,10 a ± 786,32
GIN	23,45 a ± 0,37	29,15 a ± 0,42	1230 c ± 50	5,13 ab ± 0,29	2049,38 b ± 76,02
GFAM	21,38 b ± 0,30	27,53 a ± 0,30	1300 bc ± 0	4,11 b ± 0,17	1539,38 b ± 184,18
GCWW-FAM	21,93 ab ± 0,46	28,18 a ± 0,49	1300 bc ± 0	4,86 ab ± 0,55	1541,71 b ± 244,44
GHWW-FAM	21,33 b ± 0,63	29,55 a ± 2,28	1380 b ± 100	4,55 ab ± 0,47	1202,80 b ± 174,38
GSHW-FAM	22,53 ab ± 1,05	29,83 a ± 2,21	1330 bc ± 50	5,59 a ± 0,65	1561,20 b ± 125,70
GCHM-FAM	22,10 ab ± 0,59	29,03 a ± 2,57	1330 bc ± 50	5,18 ab ± 0,85	1801,70 b ± 546,05
GPCM-FAM	21,65 b ± 0,26	28,15 a ± 0,29	1300 bc ± 0	5,04 ab ± 0,31	1977,76 b ± 356,04

Means followed by the same lower-case letter within a column are not significantly different at p < 0,05.

In contrast, the GIN geopolymer showed higher WA compared to the GFAM, GHWW-FAM, and GP-CM-FAM geopolymers and had the smallest DBD among all other geopolymer composites. These results were anticipated, considering the composition of the GFAM composite, which incorporated mineralized sawdust. However, the GIN geopolymer showed promise in terms of the HWW and PCM treatments, as these treatments improved the hygroscopic properties of their respective composites. These findings align with previous studies. For instance, Asante *et al.* (2021) investigated geopolymer composites incorporated with Eucalyptus particles and reported values of 46 % for WA, 47 % for AP, and 1030 kg/m³ for DBD. Azevedo *et al.* (2017) analyzed only geopolymer pastes without aggregates and found values close to 15 % for WA, 24 % for AP, and 1600 kg/m³ for DBD, for the same properties.

Overall, the geopolymer composites demonstrated similar MOR values, which is promising because the incorporation of sawdusts resulted in decreased weight without compromising the strength of the composites. It is important to consider that the small initial slope observed in the force vs. displacement curves for the GSAN, GIN, and GFAM composites could be attributed to the strong interlocking effect between the geopolymer matrix and the sand or sawdust particles.

However, the composites reinforced with sawdusts did exhibit smaller MOE values when compared to the GSAN composite. This reduction in MOE suggests a slight decrease in stiffness for the sawdust-reinforced composites. Besides, the decrease in MOE for the sawdust-reinforced composites might be related to the lower stiffness of the sawdust compared to sand particles. Furthermore, the smaller MOE values in sawdust-reinforced composites could also be attributed to the presence of voids or weak interfaces between the geopolymer matrix and the sawdust particles. The irregular shape and size of sawdust particles might hinder the efficient load transfer, leading to a reduction in stiffness. However, it's worth mentioning that the MOE values are still within an acceptable range for various engineering applications, and the incorporation of sawdust can offer additional benefits such as improved sustainability and reduced environmental impact.

The force vs. displacement curves depicted in Figure 6 show a small initial slope for the GSAN specimen, which is also observed for the GIN and GFAM composites. This initial slope indicates the elastic behavior of these composites before reaching their maximum load-carrying capacity. Among the sawdust-reinforced composites, there were no significantly different means for MOE, implying that the addition of sawdust did not significantly impact the overall stiffness of these composites when compared to each other.

Maderas. Ciencia y tecnología 2025 (27): 13, 1-19

Universidad del Bío-Bío
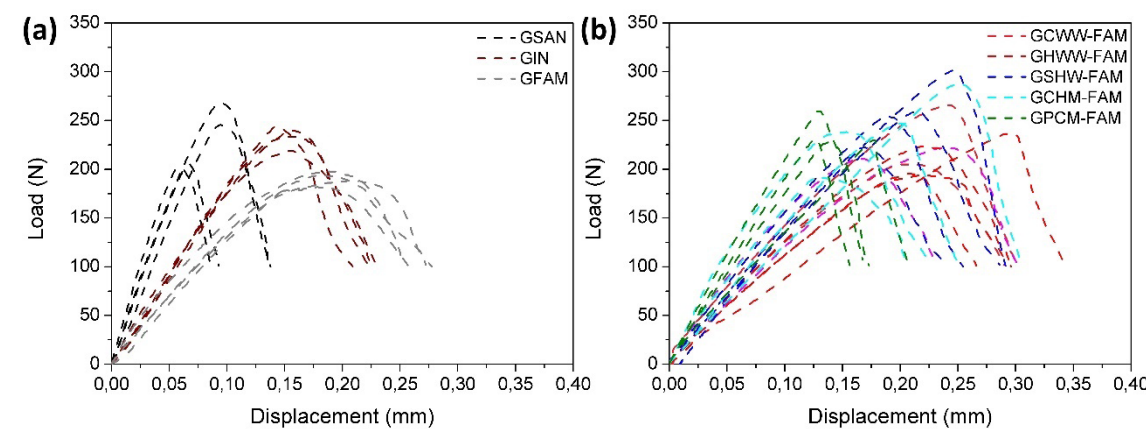
Figure 6: Bending force vs. displacement curves of the composites.

The compressive strength data for specimens at 28 days, 90 days, and after aging are presented in Table 5, wherein, in general, the compressive strength in the specimens maintained the same level from 28 to 90 days. Furthermore, all the aged specimens exhibited lower compressive strength values compared to their respective unaged counterparts, indicating that appropriate aging tests were conducted for all cases. These losses of properties can be attributed to microstructural changes induced by the aging process, such as increased porosity or the development of microcracks. It is important to note that this decrease in strength does not necessarily imply inadequate performance but rather reflects the influence of various environmental factors that can affect the material over time. Similar decreases due to aging processes were extensively reported in the literature (Arslan *et al.* 2019, Asante *et al.* 2021).

Table 5: Compressive strength of the specimens.

Specimens	28 days (MPa)	90 days (MPa)	AAT (MPa)
GSAN	19,12 abA ± 3,20	17,93 abA ± 1,41	4,17 cdC ± 1,16
GIN	20,04 abA ± 0,72	15,66 bcB ± 0,81	1,75 dD ± 0,57
GFAM	18,04 abA ± 0,69	10,90 eB ± 1,32	0,91 dD ± 0,24
GCWW-FAM	16,93 bA ± 1,24	11,71 deB ± 1,29	0,95 dD ± 0,20
GHWW-FAM	16,86 bA ± 0,76	12,20 deA ± 1,06	15,67 abA ± 6,54
GSHW-FAM	19,05 abAB ± 0,92	14,94 cB ± 0,65	23,63 aA ± 6,80
GCHM-FAM	21,50 aA ± 0,45	13,94 cdB ± 0,92	2,37 dDE ± 0,63
GPCM-FAM	21,36 aA ± 1,88	18,50 aA ± 1,44	11,18 bcB ± 2,54

Means followed by the same lower-case letter within a column and the same uppercase letter within a line are not significantly different at $p < 0,05$.

Mineralization of chemically treated sawdust..: Morais Júnior *et. al*

Maderas. Ciencia y tecnología 2025 (27): 13, 1-19

However, the GSHW-FAM composite was an exception, as it did not show a decrease in compressive strength after the aging process. This finding suggests that the sawdust treated with SHW might have delayed the geopolymerization process, and a post-cure phenomenon occurred during the aging tests in this specific case (Ye *et al.* 2018, Maichin *et al.* 2020, Asante *et al.* 2022). The lack of decreased compressive strength after aging suggests that the SHW-treated sawdust may have influenced the geopolymerization kinetics. The SHW treatment might have modified the reactivity of the sawdust or affected the pore structure within the geopolymer matrix, resulting in a delay in the geopolymerization process. Indeed, the surface layer of minerals formed on the sawdust surface can have a significant influence on the properties and behavior of the geopolymer composites. The presence of the mineral layer can enhance the bonding between the geopolymer matrix and the sawdust particles, leading to improved interfacial adhesion.

During the burning tests, it was observed that all specimens did not ignite and did not exhibit any apparent flames. As a result, the linear burning rate was found to be zero, classifying them as non-flammable materials. Although the geopolymerization process itself creates a highly cross-linked, three-dimensional structure that adds to the material's thermal stability, this characteristic can be attributed to the thermal and combustion characteristics of the FA (Kumar *et al.* 2013, Wang and Zhao 2019). The non-flammable nature of geopolymer composites containing FA ensures that these materials can withstand exposure to high temperatures and fire incidents without promoting flame spread or ignition. This property makes them suitable for use in fire-prone environments or structures where fire safety is of critical concern.

In summary, Figure 7 shows that the thermogravimetric profile consists of different stages corresponding to distinct thermal events. These stages include an initial weight loss at low temperatures (between room temperature and around 110 °C) when any moisture present in the sample evaporates, leading to an initial weight loss. Then, there is a combustion of organic components between 200 °C and 500 °C, where any organic matter undergoes combustion, resulting in a significant weight loss. After that, there is a decomposition of FA and other inorganic components, which occurs over a range of temperatures, depending on the specific composition of the geopolymers. Finally, a residual mass remains after all the volatile components have been driven off, and the thermogravimetric profile stabilizes around 700 ºC, indicating the remaining solid components or ash. This temperature at which stabilization occurs provides insights into the thermal stability of the geopolymers and can even guide the selection of geopolymers suitable for specific applications.
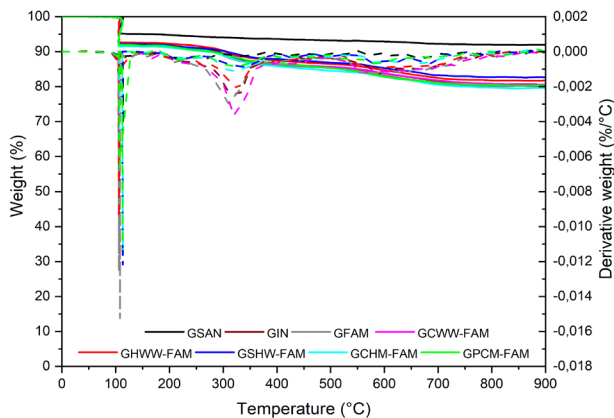

Figure 7: TG and DTG curves of the composites.

The GSAN composite presented the greatest thermal stability, especially after 110 ºC, which can be explained by its high sand content accompanied by absence of sawdust. Among the geopolymer composites incorporated with wood sawdust, those made with sawdust pretreated by SHW, CHM and PCM were more thermally stable, especially above 110 ºC. During the pretreatment processes, some of these organic components are removed or modified, leading to a reduction in their content in the sawdust.

The specimens that used sawdust showed more evident downgrades after 110 °C, especially in the 250-400 ºC and 550-700 ºC. These thermal events appeared as prominent peaks at the DTG profile. Until 110 ºC

there is only a causes a drying process, starting from the water located in the inter-cellular spaces and then degrading the hydrogen bonds that link water molecules to the hydroxyls from the wood cell wall (Yel *et al.* 2022). The peak observed around 250-400 ºC in the DTG graph of all the wood-reinforced geopolymer composites is related to the initial degradation of hemicelluloses and the beginning of lignin decomposition (Stevulova *et al.* 2014, Quiroga *et al.* 2016). On the other hand, the peak at 550-700 °C indicates the completion of the decomposition of the organic components present in the wood sawdust (Stevulova *et al.* 2014, Quiroga *et al.* 2016, Członka *et al.* 2020). At this stage, most of the hemicellulose, cellulose, and lignin have undergone thermal degradation, leaving behind primarily inorganic components, such as silica and alumina, which are typical constituents of geopolymer matrices.

The mass loss became stable after 700 °C, which is an expected mechanism based on the literature (Nath *et al.* 2016, Arslan *et al.* 2019). Up to around 700 °C, the thermal decomposition of the organic components is the dominant mechanism, and the mass loss continues steadily. However, as the temperature increases beyond 700 °C, the organic components have mostly decomposed, and their contribution to the mass loss diminishes significantly.

Based on the EDS results, the composite compounds were identified and highlighted in the SEM images shown in Figure 8. These findings were made through comparisons with SEM images obtained from previous studies (Abdullah *et al.* 2012, Sarmin and Welling 2016, Ye *et al.* 2018, Furtos *et al.* 2021, Furtos *et al.* 2022).
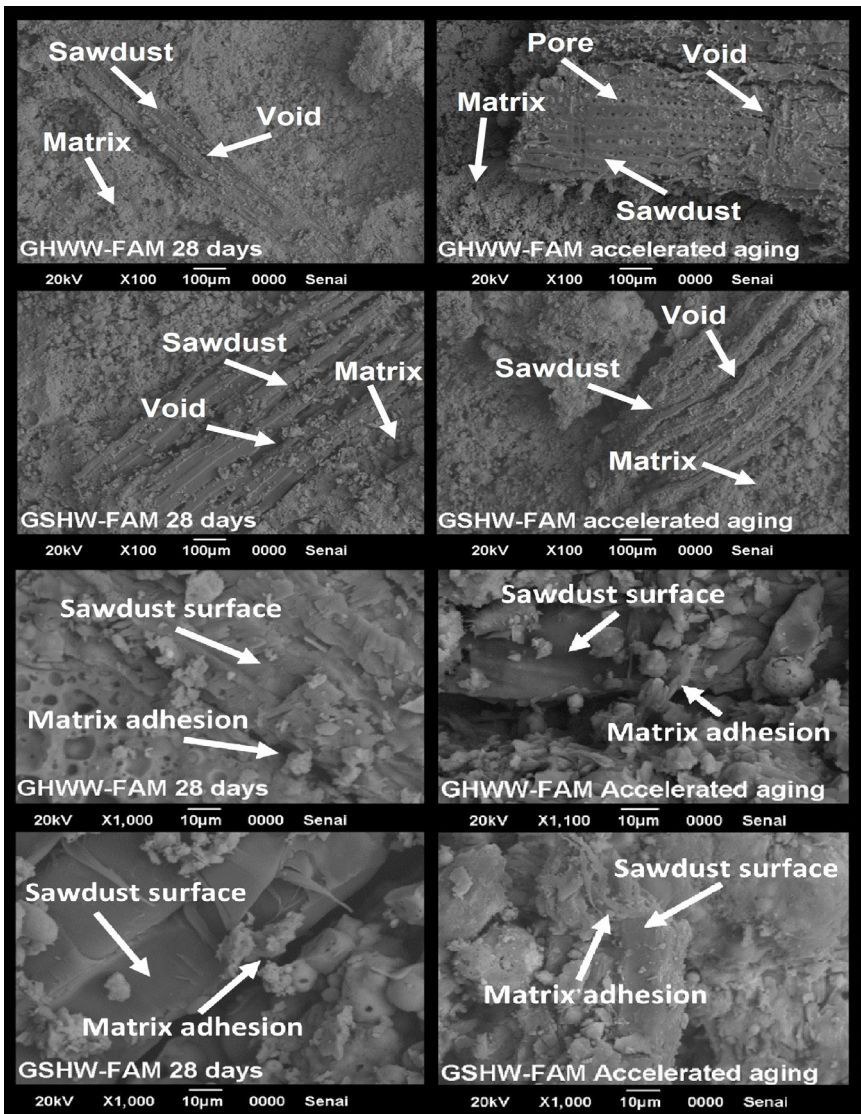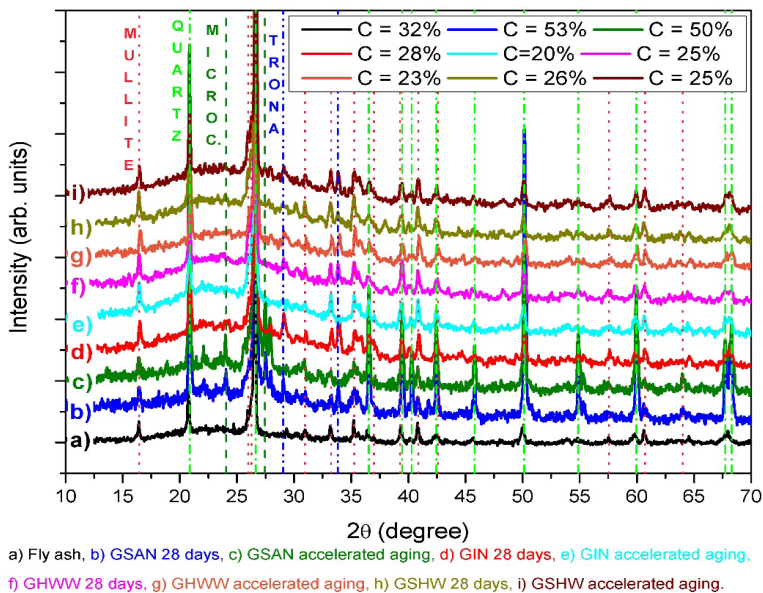

Figure 8: SEM images of the geopolymer composites acquired at low and high magnifications.

Mineralization of chemically treated sawdust..: Morais Júnior *et. al*

Maderas. Ciencia y tecnología 2025 (27): 13, 1-19

SEM images of the geopolymer composites also highlight each aggregate type to compare each other. Also, results for both the 28 days-old and aged specimens are provided. The images show that GHWW-FAM and GSHW-FAM specimens have a surface with exposed pores and voids, that allowed the attachment of small FA particles (highlighted by arrows). SEM images taken at high magnification (around 1000×) shows that the wood cell wall mineralized positively interacted with the geopolymer matrix. Probably, there was a significant adhesion between the geopolymer matrix and the wood-based aggregates (as highlighted by arrows), which explain some aforementioned mechanical properties. Also, the outstanding combustion performance shown by the composites may be ascribed to this good wood-geopolymer interface.

Figure 9 compares X-ray diffractograms of the FA and the 28 days-old and aged specimens. Again, quartz (COD 96-500-0036) and mullite (COD 96-900-1568) appear as dominant crystalline phases in all diffractograms, which is probably due to their presence of large amounts of FA.

a) Fly ash, b) GSAN 28 days, c) GSAN accelerated aging, d) GIN 28 days, e) GIN accelerated aging,
f) GHWW 28 days, g) GHWW accelerated aging, h) GSHW 28 days, i) GSHW accelerated aging.

Figure 9: XRD patterns and crystallinity index of the composites.

The formation of the trona phase (COD 96-900-7658) was observed in all geopolymer composites, but it was particularly pronounced in the composites containing sawdust. Trona (sodium sesquicarbonate) is a specific mineral phase that can form during the geopolymerization process, which is known to be associated with the reaction of sodium-based activators with aluminosilicate materials (Assaedi *et al.* 2019). In the composites containing sawdust, the formation of the trona phase can be attributed to the interaction between the wood sawdust and the alkaline activators during the geopolymerization process. Wood sawdust contains cellulose, which has hydroxyl groups that can participate in the geopolymerization reaction. The presence of cellulose in the sawdust may facilitate the formation of the trona phase, as it provides additional sites for the reaction with the alkaline activators.

The microcline phase (COD 96-900-4192), which is a potassium (K) and sodium (Na) rich alkali feldspar, was only found in GSAN composite. According to Lekshmi and Sudhakumar (2022), during the alkaline activation of the sand-rich geopolymer precursors, the alkali activators react with the silica in the sand, releasing cations like potassium (K) and sodium (Na), and these cations can then participate in the formation of various mineral phases, including the microcline phase.

XRD analysis also revealed that the GSAN geopolymer composite exhibited increased crystallinity compared to the others. This phenomenon can be attributed to the abundant silica provided by sand since the availability of silicon (Si) promotes the formation of crystalline phases, including microcline and other crystalline components. On the other hand, the higher sand content also yielded a reduction in mullite content within the geopolymer composites. Mullite is a desirable phase known for enhancing mechanical properties and thermal stability in geopolymers. The decrease in mullite content can be attributed to the dominance of

Maderas. Ciencia y tecnología 2025 (27): 13, 1-19

Universidad del Bío-Bío

other crystalline phases, particularly microcline, favored by the higher sand content.

Compared to the GSAN composite, it was clear that the incorporation of sawdust in geopolymer composites induces a reduction in crystallinity. This behavior is attributed to the organic components present in sawdust, such as cellulose and lignin. During the geopolymerization process, these organic components act as diluents, hindering the formation of crystalline phases (Furtos *et al.* 2021, Olayiwola *et al.* 2021). Furthermore, there were differences in the characteristic amorphous regions (halos) between the FA and the geopolymerized specimens. The FA sample (a) exhibited an amorphous halo in the angular range of 17° to 32°, whereas the specimens containing sawdust (d, e, f, g, h) display a broader and higher amorphous region, spanning from 16° to 33°.

The aged GSHW-FAM specimen (i) stood out with the highest and widest amorphous region, while the GSAN sand specimens (b, c) showed an amorphous halo similar to that of the original FA, indicating a lower amount of amorphous content. As reported by Furtos *et al.* (2022) and Rattanasak and Chindaprasirt (2009), this enlargement of the amorphous halo suggests a highly disordered diffusion of the glassy aluminosilicate structure within the polymeric network, confirming the formation of an amorphous aluminosilicate gel.

CONCLUSIONS

In conclusion, geopolymer composites GHWW-FAM and GSHW-FAM exhibited similar and improved properties compared to those made with sand, offering the added advantage of lower density. These lightweight composites demonstrate significant potential for diverse engineering applications, particularly by utilizing abundant industrial waste and enabling cost-effective production. Despite a slight reduction in stiffness, the sawdust-reinforced composites maintained satisfactory MOR values, highlighting their ability to withstand substantial loads without fracturing.

The compressive strength data confirmed the suitability of these geopolymer composites for construction materials, showing substantial strength development between 28 and 90 days. The observed decrease in compressive strength in aged specimens is a typical characteristic of geopolymer materials, providing valuable insights into their long-term behavior. The exceptional performance of the GSHW-FAM composite underscores the critical role of sawdust treatments in influencing geopolymerization kinetics, meriting further research.

Futhermore, the non-flammable properties of these composites make them ideal for applications in the transportation industry, particularly in railways and aviation, where stringent fire safety regulations are mandatory. They can also be employed in construction of fire-resistant walls, panels, and insulation materials, enhancing building safety and reducing fire propagation risks

Understanding the influence of various additives and treatments on the geopolymerization process is essential for optimizing the properties and performance of these composites across a wide range of engineering applications. By capitalizing on their inherent strengths and fire-resistant characteristics, geopolymer composites hold great promise for addressing engineering challenges while promoting sustainable materials in the construction and transportation industries.

Authorship contributions

R. R. M. J.: Conceptualization, software, validation, formal analysis, investigation, data curation, writing—original draft preparation. A. B. A.: Conceptualization, software, validation, writing—original draft preparation. A. L. M.o: Methodology, formal analysis, Writing—review and editing, supervision. R. A. D.s: Methodology, investigation, writing—original draft preparation, writing-review and editing, supervision, funding acquisition. D. A. G.: Methodology, software, resources, supervision, writing—review and editing, visualization, project administration, funding acquisition. R. B.: Writing—review and editing, visualization, funding acquisition.

Mineralization of chemically treated sawdust..: Morais Júnior *et. al*

Maderas. Ciencia y tecnología 2025 (27): 13, 1-19

Acknowledgements

REFERENCES

ABNT. 2005. Agregados para concreto - Especificação. ABNT NBR 7211. ABNT: Rio de Janeiro, Brazil.

ABNT. 2005. Agregados para concreto - Especificação. ABNT NBR 7211: ABNT: Rio de Janeiro, Brazil.

ABNT. 2006. Agregados - Determinação da massa unitária e do volume de vazios. ABNT NBR NM 45-06. ABNT: Rio de Janeiro, Brazil.

ABNT. 2019. Cimento Portland - Determinação da resistência à compressão de corpos de prova cilíndricos. ABNT NBR 7215. ABNT: Rio de Janeiro, Brazil.

Ahmaruzzaman, M. 2010. A Review on the utilization of fly ash. *Progress in Energy and Combustion Science* 36(3): 327-363. https://doi.org/10.1016/j.pecs.2009.11.003

Abdullah, M.M.A.; Ahmad, M.I.; Faheem, M.T.M.; Kamarudin, H.; Nizar, K.I.; Bnhussain, M.; Rafiza, A.R.; Zarina, Y.; Liyana, J. 2012. Feasibility of producing wood fibre-reinforced geopolymer composites (WFRGC). *Advanced Materials Research* 626: 918-925. https://doi.org/10.4028/www.scientific.net/AMR.626.918

Amran, M.; Debbarma, S.; Ozbakkaloglu, T. 2021. Fly ash-based eco-friendly geopolymer concrete: a critical review of the long-term durability properties. *Construction and Building Materials* 270. 121857. https://doi.org/10.1016/j.conbuildmat.2020.121857

Amran, Y.H.M.; Alyousef, R.; Alabduljabbar, H.; El-Zeadani, M. 2020. Clean production and properties of geopolymer concrete: a review. *Journal of Cleaner Production* 251(April). e119679. https://doi.org/10.1016/j.jclepro.2019.119679

Arslan, A.A.; Uysal, M.; Yılmaz, A.; Al-mashhadani, M.M.; Canpolat, O.; Şahin, F.; Aygörmez, Y. 2019. Influence of wetting-drying curing system on the performance of fiber reinforced metakaolin-based geopolymer composites. *Construction and Building Materials* 225: 909-926. https://doi.org/10.1016/j.conbuildmat.2019.07.235

Asante, B.; Schmidt, G.; Teixeira, R.; Krause, A.; Savastano-Junior, H. 2021. Influence of wood pre-treatment and fly ash particle size on the performance of geopolymer wood composite. *European Journal of Wood and Wood Products* 79(3): 597-609. https://doi.org/10.1007/s00107-021-01671-9

Asante, B.; Ye, H.; Nopens, M.; Schmidt, G.; Krause, A. 2022. Influence of wood moisture content on the hardened state properties of geopolymer wood composites. *Composites Part A: Applied Science and Manufacturing* 152. e106680. https://doi.org/10.1016/j.compositesa.2021.106680

Assaedi, H.; Alomayri, T.; Shaikh, F.; Low, I.M. 2019. Influence of nano silica particles on durability of flax fabric reinforced geopolymer composites. *Materials* 12(9). e1459. https://doi.org/10.3390/ma12091459

ASTM International. ASTM. 1999. Standard test methods for flexural properties of ceramic whiteware materials. ASTM C674-99. ASTM International: West Conshohocken, PA, USA.

ASTM International. ASTM 2023. Standard practice for operating fluorescent ultraviolet (UV) lamp apparatus for exposure of materials. ASTM G154-23. ASTM International: West Conshohocken, PA, USA.

Azevedo, A.G.S.; Strecker, K.; Araújo Jr., A.G.; Silva, C.A. 2017. Produção de geopolímeros à base de cinza volante usando soluções ativadoras com diferentes composições de Na_2O e Na_2SiO_3. *Cerâmica* 63(366): 143-151. https://doi.org/10.1590/0366-69132017633662078

Maderas. Ciencia y tecnología 2025 (27): 13, 1-19

Universidad del Bío-Bío

Boadu, K.B.; Antwi-Boasiako, C.; Ofosuhene, L. 2018. Solvent extraction of inhibitory substances from three hardwoods of different densities and their compatibility with cement in composite production. *Journal of the Indian Academy of Wood Science* 15(2): 140-148. https://doi.org/10.1007/s13196-018-0219-0

Cardoso, A.M.; Paprocki, A.; Ferret, L.S.; Azevedo, C.M.N.; Pires, M. 2015. Synthesis of zeolite Na-Pl under mild conditions using Brazilian coal fly ash and its application in wastewater treatment. *Fuel* 139: 59-67. https://doi.org/10.1016/j.fuel.2014.08.016

Członka, S.; Strąkowska, A.; Pospiech, P.; Strzelec, K. 2020. Effects of chemically treated eucalyptus fibers on mechanical, thermal and insulating properties of polyurethane composite foams. *Materials* 13(7). e1781. https://doi.org/10.3390/ma13071781

Danish, A.; Ozbakkaloglu, T.; Ali Mosaberpanah, M.; Salim, M.U.; Bayram, M.; Yeon, J.H.; Jafar, K. 2022. Sustainability benefits and commercialization challenges and strategies of geopolymer concrete: a review. *Journal of Building Engineering* 58. e105005. https://doi.org/10.1016/j.jobe.2022.105005

Fan, M.; Ndikontar, M.K.; Zhou, X.; Ngamveng, J.N. 2012. Cement-bonded composites made from tropical woods: compatibility of wood and cement. *Construction and Building Materials* 36: 135-140. https://doi.org/10.1016/j.conbuildmat.2012.04.089

Furtos, G.; Molnar, L.; Silaghi-Dumitrescu, L.; Pascuta, P.; Korniejenko, K. 2022. Mechanical and thermal properties of wood fiber reinforced geopolymer composites. *Journal of Natural Fibers* 19(13): 6676-6691. https://doi.org/10.1080/15440478.2021.1929655

Furtos, G.; Silaghi-Dumitrescu, L.; Pascuta, P.; Sarosi, C.; Korniejenko, K. 2021. Mechanical properties of wood fiber reinforced geopolymer composites with sand addition. *Journal of Natural Fibers* 18(2): 285-296. https://doi.org/10.1080/15440478.2019.1621792

Garcez, M. R.; Santos, T.; Garcez, E. O.; Gatto, D. 2016. Propriedades mecânicas de compósitos cimento-madeira com serragem tratada de Pinus elliottii. *Revista Ciência da Madeira* 7(1): 16-27. https://doi.org/10.12953/2177-6830/rcm.v7n1p16-27

Gollakota, A.R.K.; Volli, V.; Shu, C.M. 2019. Progressive utilisation prospects of coal fly ash: a review. *Sci Total Environ* 672: 951-989. https://doi.org/10.1016/j.scitotenv.2019.03.337

Jorge, F.C.; Pereira, C.; Ferreira, J.M.F. 2004. Wood-cement composites: a review. *Holz als Roh- und Werkstoff* 62(5): 370-377. https://doi.org/10.1007/s00107-004-0501-2

Kumar, M.; Kumar, M.; Arora, S. 2013. Thermal degradation and flammability studies of wood coated with fly ash intumescent composites. *Journal of the Indian Academy of Wood Science* 10(2): 125-133. https://doi.org/10.1007/s13196-013-0105-8

Lazorenko, G.; Kasprzhitskii, A.; Yavna, V.; Mischinenko, V.; Kukharskii, A.; Kruglikov, A.; Kolodina, A.; Yalovega, G. 2020. Effect of pre-treatment of flax tows on mechanical properties and microstructure of natural fiber reinforced geopolymer composites. *Environmental Technology & Innovation* 20. e101105. https://doi.org/10.1016/j.eti.2020.101105

Lekshmi, S.; Sudhakumar, J. 2022. An assessment on the durability performance of fly ash-clay based geopolymer mortar containing clay enhanced with lime and GGBS. *Cleaner Materials* 5. e100129. https://doi.org/10.1016/j.clema.2022.100129

Luhar, I.; Luhar, S. 2022. A Comprehensive review on fly ash-based geopolymer. *Journal of Composites Science* 6(8). e219. https://doi.org/10.3390/jcs6080219

Maichin, P.; Suwan, T.; Jitsangiam, P.; Chindaprasirt, P. 2020. Hemp fiber reinforced geopolymer composites: effects of naoh concentration on fiber pre-treatment process. *Key Engineering Materials* 841: 166-170. https://doi.org/10.4028/www.scientific.net/KEM.841.166

Maichin, P.; Suwan, T.; Jitsangiam, P.; Chindaprasirt, P.; Fan, M. 2020. Effect of self-treatment process on properties of natural fiber-reinforced geopolymer composites. *Materials and Manufacturing Processes* 35(10): 1120-1128. https://doi.org/10.1080/10426914.2020.1767294

Mineralization of chemically treated sawdust..: Morais Júnior *et. al*

Maderas. Ciencia y tecnología 2025 (27): 13, 1-19

Malenab, R.; Ngo, J.; Promentilla, M. 2017. Chemical treatment of waste abaca for natural fiber-reinforced geopolymer composite. *Materials* 10(6). e579. https://doi.org/10.3390/ma10060579

Manique, M.C.; Lacerda, L.V.; Alves, A.K.; Bergmann, C.P. 2017. Biodiesel production using coal fly ash-derived sodalite as a heterogeneous catalyst. *Fuel* 190: 268-273. https://doi.org/10.1016/j.fuel.2016.11.016

Nath, S.K.; Maitra, S.; Mukherjee, S.; Kumar, S. 2016. Microstructural and morphological evolution of fly ash based geopolymers. *Construction and Building Materials* 111: 758-765. https://doi.org/10.1016/j.conbuildmat.2016.02.106

Olayiwola, H.O.; Amiandamhen, S.O.; Meincken, M.; Tyhoda, L. 2021. Investigating the suitability of fly ash/metakaolin-based geopolymers reinforced with south african alien invasive wood and sugarcane bagasse residues for use in outdoor conditions. *European Journal of Wood and Wood Products* 79(3): 611-627. https://doi.org/10.1007/s00107-020-01636-4

Pavithra, P.; Srinivasula Reddy, M.; Dinakar, P.; Hanumantha Rao, B.; Satpathy, B.K.; Mohanty, A.N. 2016. A mix design procedure for geopolymer concrete with fly ash. *Journal of Cleaner Production* 133: 117-125. https://doi.org/10.1016/j.jclepro.2016.05.041

Quiroga, A.; Marzocchi, V.; Rintoul, I. 2016. Influence of Wood Treatments on Mechanical properties of wood-cement composites and of populus euroamericana wood fibers. *Composites Part B: Engineering* 84: 25-32. https://doi.org/10.1016/j.compositesb.2015.08.069

Ranjbar, N.; Zhang, M. 2020. Fiber-reinforced geopolymer composites: a review. *Cement and Concrete Composites* 107. e103498. https://doi.org/10.1016/j.cemconcomp.2019.103498.

Rattanasak, U.; Chindaprasirt, P. 2009. Influence of NaOH solution on the synthesis of fly ash geopolymer. *Minerals Engineering* 22(12): 1073-1078. https://doi.org/10.1016/j.mineng.2009.03.022

Ravindran, R.; Jaiswal, A.K. 2016. A comprehensive review on pre-treatment strategy for lignocellulosic food industry waste: Challenges and opportunities. *Bioresource Technology* 199: 92-102. https://doi.org/10.1016/j.biortech.2015.07.106

Sarmin, S.N.; Welling, J. 2016. Lightweight geopolymer wood composite synthesized from alkali-activated fly ash and metakaolin. *Jurnal Teknologi* 78(11): 49-55. https://doi.org/10.11113/.v78.8734

Sciban, M.; Klasnja, M.; Skrbic, B. 2006. Modified softwood sawdust as adsorbent of heavy metal ions from water. *Journal of Hazardous Materials* 136(2): 266-271. https://doi.org/10.1016/j.jhazmat.2005.12.009

Stevulova, N.; Cigasova, J.; Estokova, A.; Terpakova, E.; Geffert, A.; Kacik, F.; Singovszka, E.; Holub, M. 2014. Properties characterization of chemically modified hemp hurds. *Materials* 7(12): 8131-8150. https://doi.org/10.3390/ma7128131

Tchadjie, L.N.; Ekolu, S.O. 2018. Enhancing the reactivity of aluminosilicate materials toward geopolymer synthesis. *Journal of Materials Science* 53(4): 4709-4733. https://doi.org/10.1007/s10853-017-1907-7

Wang, Y.; Zhao, J. 2019. Facile preparation of slag or fly ash geopolymer composite coatings with flame resistance. *Construction and Building Materials* 203: 655-661. https://doi.org/10.1016/j.conbuildmat.2019.01.097

Yang, J.; Huang, J.; Su, Y.; He, X.; Tan, H.; Yang, W.; Strnadel, B. 2019. Eco-friendly treatment of low-calcium coal fly ash for high pozzolanic reactivity: a step towards waste utilization in sustainable building material. *Journal of Cleaner Production* 238. e117962. https://doi.org/10.1016/j.jclepro.2019.117962

Ye, H.; Zhang, Y.; Yu, Z.; Mu, J. 2018. Effects of cellulose, hemicellulose, and lignin on the morphology and mechanical properties of metakaolin-based geopolymer. *Construction and Building Materials* 173: 10-16. https://doi.org/10.1016/j.conbuildmat.2018.04.028

Yel, H.; He, C.; Urun, E. 2022. Performance of cement-bonded wood particleboards produced using fly ash and spruce planer shavings. *Maderas. Ciencia y Tecnología* 24. e44. https://doi.org/10.4067/S0718-221X2022000100444